Knockdown of fast skeletal myosin-binding protein C in zebrafish results in a severe skeletal myopathy

Mei Li,[1] Monika Andersson-Lendahl,[2] Thomas Sejersen,[3] and Anders Arner[1]

[1]Department of Physiology and Pharmacology, [2]Department of Cell and Molecular Biology, and [3]Department of Women's and Children's Health, Karolinska Institutet, SE 171 77 Stockholm, Sweden

Myosin-binding protein C (MyBPC) in the muscle sarcomere interacts with several contractile and structural proteins. Mutations in the cardiac isoform (MyBPC-3) in humans, or animal knockout, are associated with cardiomyopathy. Function of the fast skeletal isoform (MyBPC-2) in living muscles is less understood. This question was addressed using zebrafish models, combining gene expression data with functional analysis of contractility and small-angle x-ray diffraction measurements of filament structure. Fast skeletal MyBPC-2B, the major isoform, was knocked down by >50% using morpholino antisense nucleotides. These morphants exhibited a skeletal myopathy with elevated apoptosis and up-regulation of factors associated with muscle protein degradation. Morphant muscles had shorter sarcomeres with a broader length distribution, shorter actin filaments, and a wider interfilament spacing compared with controls, suggesting that fast skeletal MyBPC has a role in sarcomere assembly. Active force was reduced more than expected from the decrease in muscle size, suggesting that MyBPC-2 is required for optimal force generation at the cross-bridge level. The maximal shortening velocity was significantly increased in the MyBPC-2 morphants, but when related to the sarcomere length, the difference was smaller, reflecting that the decrease in MyBPC-2B content and the resulting myopathy were accompanied by only a minor influence on filament shortening kinetics. In the controls, equatorial patterns from small-angle x-ray scattering revealed that comparatively few cross-bridges are attached (as evaluated by the intensity ratio of the 11 and 10 equatorial reflections) during active contraction. X-ray scattering data from relaxed and contracting morphants were not significantly different from those in controls. However, the increase in the 11:10 intensity ratio in rigor was lower compared with that in controls, possibly reflecting effects of MyBPC on the cross-bridge interactions. In conclusion, lack of MyBPC-2 results in a severe skeletal myopathy with structural changes and muscle weakness.

INTRODUCTION

Myosin-binding protein C (MyBPC) is a sarcomeric protein in muscle, originally discovered in 1973 (Offer et al., 1973). The protein exists in three main isoforms (Bennett et al., 1999; Winegrad, 1999), skeletal slow (MyBPC-1), skeletal fast (MyBPC-2), and cardiac (MyBPC-3). The structure and function of the cardiac isoform have received significant attention, triggered by early reports that mutations in the MyBPC-3 gene are associated with cardiomyopathy (Bonne et al., 1995; Watkins et al., 1995). The MyBPC-3 molecule consists of 11 domains (C0–C10) where the C-terminal domains (C9–C10) are reported to interact with the thick myosin filament and titin and the N-terminal C0–C1 binds to actin and the myosin head region. There are three main serine phosphorylation sites in a linker domain between the C1 and C2 domains (Gautel et al., 1995; Gruen et al., 1999; Kunst et al., 2000; Finley and Cuperman, 2014). The protein has several putative functions, e.g., contributing to filament formation and stability (Freiburg and Gautel, 1996; Van Der Ven et al., 1999), tethering

myosin heads to the thick filament backbone, affecting cross-bridge kinetics and Ca^{2+} sensitivity (Kunst et al., 2000; Kulikovskaya et al., 2003; Harris et al., 2004). Phosphorylation of MyBPC-3 (Gautel et al., 1995), mainly via protein kinase A, has been shown to affect the interaction of the N-terminal regions with actin and myosin (Weisberg and Winegrad, 1996; Colson et al., 2012), thereby providing an important regulatory mechanism in the heart.

Previous research on MyBPC has mainly focused on the cardiac isoform. This most likely reflects the prominent clinical implications, but also the availability of transgenic mouse models (Yang et al., 1998; Witt et al., 2001; Harris et al., 2002; Sadayappan et al., 2005; Michalek et al., 2013). Although MyBPC was originally identified in skeletal muscle and pioneering work on its function was done in skeletal muscle fibers (Craig and Offer, 1976; Hofmann et al., 1991b), information on the function of the skeletal isoforms is much less. The first skeletal MyBP-C cDNA was reported by Fürst

The Rockefeller University Press $30.00
J. Gen. Physiol. Vol. 147 No. 4 309–322
www.jgp.org/cgi/doi/10.1085/jgp.201511452

309

et al. (1992). The skeletal MyBPC isoforms lack the N-terminal C0 domain, two of the three phosphorylation sites, and a proline-rich insert in the C5 domain (Oakley et al., 2004), compared with the cardiac isoform. Skeletal MyBPC has been shown to bind in the sarcomere in a similar manner as the cardiac isoform (Freiburg and Gautel, 1996; Gilbert et al., 1999; Luther et al., 2008), and MyBPC-1 has been shown to undergo phosphorylation (Ackermann and Kontrogianni-Konstantopoulos, 2011).

Recently, mutations in slow skeletal MyBPC-1 have been linked to skeletal myopathy (Gurnett et al., 2010; Markus et al., 2012), and mRNA injection of mutated MyBPC-1 in zebrafish has been shown to induce structural defects in muscle (Ha et al., 2013). To our knowledge, the fast skeletal MyBPC-2 has not been linked to disease, and no specific transgenic mouse models are available.

The objective of this study was to investigate the function of the skeletal MyBPC isoforms and potential association with skeletal myopathy. For this purpose, we applied a structural/functional approach in the zebrafish larval model (Dou et al., 2008; Li et al., 2013), analyzed the expression of all MyBPC isoforms in the skeletal muscle, and knocked down the fast skeletal MyBPC isoform, which resulted in a severe myopathy. Using this model, we addressed questions regarding the role of the fast skeletal MyBPC during sarcomere development, in the sarcomere structure, and on the cross-bridge interaction.

MATERIALS AND METHODS

Animals and preparation
Zebrafish (TU strain) were maintained at the Karolinska Institutet zebrafish facility at the Department of Cell and Molecular Biology. Embryos were obtained using natural mating. Morpholino antisense oligonucleotide (MO) injections were performed on 1–2-cell-stage embryos. The larvae included in this study were 4–6 d postfertilization (dpf). They were anesthetized using 0.02% MS-222 (tricaine methanesulfonate; Sigma-Aldrich) before experiments. All experiments were performed according to European guidelines for animal research, complied with national regulations for the care of experimental animals, and were approved by the local animal ethics committee.

Design and injection of MOs
We identified three MyBPC skeletal isoforms (*mybpc-1*, *mybpc-2a*, and *mybpc-2b*) in the zebrafish genome and obtained both splicing and translation blocking MOs (Gene Tools) as shown in Table S1. For comparison, we used a standard control MO (5′-CCTCTTACCT-CAGTTACAATTTATA-3′; Gene Tools).

Quantitative PCR (qPCR) and protein analysis
RNA was purified from somite regions of wild-type larvae (RNeasy kit; QIAGEN). Using qPCR, we quantified the expression of all MyBPC isoforms in zebrafish skeletal muscles at 1, 4, and 7 dpf, respectively (QuantiTect SYBR green RT-PCR kit; QIAGEN). The primers used for each gene are listed in Table S1. To determine

the extent of knockdown, RNA was extracted from splicing blocking morphants at 4 dpf, reverse transcribed (QuantiTect Reverse Transcription kit; QIAGEN), and amplified by PCR using the following forward (*mybpc-1*, 5′-ATAACGTAGCGCTGGACTGG-3′; *mybpc-2a*, 5′-TTGTGGAGAGGCCTCAGACT-3′; *mybpc-2b*, 5′-AGAAACCAGAGCCTGAGCTG-3′) and reverse (*mybpc-1*, 5′-TCT-GTGAAGTCGCGGTCATT-3′; *mybpc-2a*, 5′-CCATCCACGACCT-TAACGAT-3′; *mybpc-2b*, 5′-TTAGGATCTGCCACCTCCAC-3′) primers. β-Actin (*Danio rerio*) was used as a standard (forward, 5′-CCCAGACATCAGGGAGTGAT-3′; reverse, 5′-TCTCTGTTG-GCTTTGGGATT-3′). The RT-PCR products were separated on 2% agarose gels and visualized using GelRed Nucleic Acid Gel Stain (Biotium) on a Bio-Rad Laboratories system. Primers used for analyses of protein degradation signaling are given in Table S2. Proteins were extracted from the somite regions of 20 larvae using a homogenization buffer as described previously (Li et al., 2013). Protein extracts were separated on 7% separation polyacrylamide gels, and the fast MyBPC-2 was identified with Western blotting using a mouse monoclonal antibody from D.O. Fürst (Institute for Cell Biology, University of Bonn, Bonn, Germany; Gautel et al., 1998). The MyBPC-2 band (molecular mass ∼130 kD) and glyceraldehyde 3-phosphate dehydrogenase band (anti-GAPDH; sc-25778; Santa Cruz Biotechnology, Inc.) were visualized using an Enhanced Chemiluminescence kit (Clarity Western ECL Substrate; Bio-Rad Laboratories).

Morphology and immunohistochemistry
For general phenotyping, the larvae were anesthetized at 4 dpf and examined using light microscopy. For muscle morphology and measurement of actin filament length, the larvae were fixed in 4% PFA at 4°C overnight and stained with rhodamine phalloidin and examined as whole-mount preparations. To examine the extent of fibrosis, fixed preparations were embedded in O.C.T. (Tissue-Tek; VWR), freeze sectioned, and stained with 0.1% Sirius red (Westerfield, 2000). Immunohistochemistry was performed on frozen sections using antibodies against slow/fast myosin heavy chain (S58, mouse anti–slow myosin/F59, mouse anti–fast myosin, 1:200; Developmental Studies Hybridoma Bank). These sections were also used for determination of muscle cross-sectional area. 1-dpf larvae were stained with Acridine orange to detect apoptosis as previously described (Furutani-Seiki et al., 1996). Confocal images were obtained using an LSM 510 microscope (ZEISS).

Mechanical analysis
Larval preparations were mounted using aluminum clips between a force transducer and a puller for rapid length changes in a MOPS-buffered solution at 22°C as described previously (Dou et al., 2008; Li et al., 2013). The preparations contained the trunk muscles, and isometric force was recorded along the long axis of the preparation. The preparations were mounted at slack length and then stimulated (single twitches) with 0.5-ms duration electrical pulses (supramaximal voltage) at 2-min intervals via two platinum electrodes placed on both sides of the preparation. To determine the length-force relationship, length was increased in steps between the contractions, from the slack length to a length above that giving maximal for active force. At each length, active and passive force was recorded. For each preparation, the optimal length (L_{opt}) for active force was determined. We also determined the time to reach half-maximal contraction and relaxation and the latency between stimulus and onset of contraction in the single twitches at L_{opt}.

The tetanus/single twitch ratio is very low compared with mammalian muscles, and the earlier phases of the tetanus are more affected by an inhibitor of fast myosin (Dou et al., 2008). The later phases of a tetanic contraction in the zebrafish larvae might thus involve fatiguing of the fast muscle and possibly recruitment of a small component of contracting slow muscle fibers. We therefore

considered it important to estimate the shortening velocity during the early phases of contraction and attempted determinations during single twitch contractions. To improve resolution, these experiments were performed at 15°C. Because the single twitch contractions are transient and very rapid in the zebrafish larvae (peak of contraction reached within ∼10 ms), we could not apply load clamp or velocity ramps under steady-state conditions, nor use the slack test method (Edman, 1979), which would require constant velocity during the shortening period. It was impossible to load clamp the preparations sufficiently fast to resolve shortening responses in the millisecond time scale at the peak. We thus developed a protocol where we initiated a shortening ramp ∼80 ms before the single twitch stimulation. A series of single twitch contractions (five to seven, at 2-min intervals) with different ramp velocities were examined. The muscles were prestretched before each stimulus, so that muscle length at the peak of the single twitch was the same (i.e., at L_{opt}) for all ramp velocities. The ramp continued for 300 ms, ∼200 ms after the peak of the single twitch contraction. The muscles where returned to the initial length in the relaxed state between stimuli. For each contraction, the velocity (V) and the corresponding peak force (P) were determined. Between each iso-velocity contraction, an isometric contraction was recorded to determine the isometric tension (P_0). To estimate stiffness, muscle length was oscillated at 1 kHz (0.1% of L_{opt}), and the resulting force responses (ΔP) were recorded and related to the length amplitude (ΔL) and the isometric tension (P_0). Stiffness values recorded in the relaxed muscles were subtracted, and stiffness at the peak of an isometric contraction was expresses as $\Delta P/(\Delta L * P_0)$.

X-ray diffraction measurements

Small-angle x-ray diffraction was performed at beamline A2, HASYLAB/DESY, Germany, and the beamline I911-SAXS, MAX IV Laboratory, Sweden, as described previously (Li et al., 2013). Larval preparations were mounted in the standard MOPS-buffered solution for measurements at 22°C and stretched to L_{opt} for active force. Solutions with different osmolarities were obtained by reducing NaCl (lower osmolarity) or adding sucrose (higher osmolarity) to the solution. Rigor was induced by adding 2 mM NaCN for 45 min. The equatorial patterns were recoded using 1–5-s exposures, and when several recordings were made on one larva, it was moved between exposures. To examine the contraction-related changes in the intensity ratio of 1.1 and 1.0 equatorial reflections, the muscles were stimulated at 200 Hz for 200 ms. In total, 15 contractions were applied. During each contraction cycle, the beam shutter was opened and the detector activated. This gave a total recoding time of 3 s, enabling determination of the intensities of 1.1 and 1.0 reflection in the relaxed or contracting (200 ms tetanus) states. A polynomial function was fitted to determine the background of the equatorial pattern, and the integrated intensity of the 1.1 and 1.0 reflections was determined.

Statistics

All data are presented as mean ± SEM. Statistical analysis and curve fitting were performed using Sigma plot 8.0 for Windows and SigmaStat for Windows 3.0 (Systat Software, Inc.). Statistical comparisons were made using Student's t test or ANOVA when more than two groups were compared.

Online supplemental material

Fig. S1 shows staining for fibrosis and myosin isoforms in control and MyBPC-2B morphants. Fig. S2 shows original recordings of force responses and length ramps in experiments determining shortening kinetics. Fig. S3 shows gross morphology of a control and a translation blocking MyBPC-2B morphant larva. Table S1 shows genes, primers, and MO sequences. Table S2 shows primers for determination of factors involved in protein degradation. Online supplemental material is available at http://www.jgp.org/cgi/content/full/jgp.201511452/DC1.

RESULTS

Three isoforms of MyBPC, with the fast isoform MyBPC-2B being the dominant

We identified three MyBPC isoforms in the zebrafish genome. The corresponding genes are shown in Table S1, including a cardiac (*mybpc-3*), a slow (*mybpc-1*), and two fast (*mybpc-2a* and *2b*) genes. We examined, using qPCR, the temporal expression (at 1, 4, and 7 dpf) of these isoforms in the trunk skeletal muscles using the primer pairs shown in Table S1. As seen in Fig. 1, the *mybpc-2b* was the dominating isoform at all examined time points. The cardiac (*mybpc-3*) and the fast type 2A (*mybpc-2a*) were expressed at very low levels. A significant expression of the slow isoform (*mybpc-1*) was detected. The *mybpc-2b* was expressed at high levels already at 1 dpf, whereas the slow type (*mybpc-1*) appeared at later time points. For both *mybpc-2b* and *mybpc-1*, the expression pattern remained unchanged between 4 and 7 dpf.

Knockdown of MyBPC isoforms using MOs

To produce morphant larvae for the MyBPC isoforms in zebrafish, we injected splicing and translation blocking MOs for each MyBPC skeletal isoform (MyBPC-1, 2A, and 2B), shown in Table S1. The MO-injected larvae are denoted morphants. We focused our analysis on the
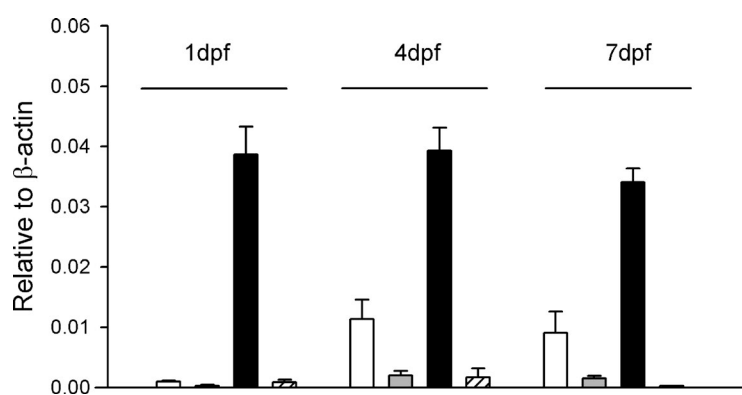
Figure 1. Expression of MyBPC variants in zebrafish larvae. Real-time qPCR of MyBPC isoforms at 1, 4, and 7 dpf in larval trunk muscles of wild-type zebrafish (open bars: *mybpc-1*, gray bars: *mybpc-2a*, black bars: *mybpc-2b*, hatched bars: *mybpc-3*). Data are shown relative to β-actin ($n = 6$–8).

splicing blocking morphants, and unless otherwise stated, morphants refer to the group injected of splicing blocking MOs. Fig. 2 A shows representative gels separating RT-PCR transcripts using primers for MyBPC-2B from 4-dpf larval trunk muscles. For each group, we included two individual samples on separate adjacent lanes. The MyBPC-2B transcript is observed in the control-injected larvae (lanes b) and remained essentially unchanged after injection of splicing MOs for the slow (*mybpc-1*, lanes c) and for the fast skeletal MyBPC-2A (lanes d) types. Injection with MO for the MyBPC-2B resulted in a marked decrease in the mRNA levels (lanes e) and the appearance of a weak band with a smaller size (broken arrow). The MO injections did not affect the mRNA expression of β-actin (Fig. 2 B). The intensities of the bands were quantified, and Fig. 2 D depicts the summarized data showing ∼80% decrease in MyBPC-2B expression after injection of the MyBPC-2B MO. We separated protein extracts from the trunk muscles on SDS-PAGE gels to confirm that the decrease in mRNA was associated with a decrease in protein. We used Western blot analysis and a monoclonal antibody against MyBPC-2 and show that the MyBPC-2 protein was significantly reduced in the MyBPC-2 morphant (to ∼50%, normalized to GAPDH; Fig. 2 C). The results show that the lowering of MyBPC-2B mRNA after MO injection is accompanied by a marked decrease in protein level. Injection of MOs for MyBPC-1 and MyBPC-2A partially (20–25%) lowered the MyBPC-2B mRNA expression (Fig. 2 D). Because the expression of the MyBPC-2A type was very low (Fig. 1), we did not perform an extensive analysis on the effects of MO injection for this type. We confirmed, however, that the MyBPC-2A mRNA remained very low after injection of the MyBPC-2B MOs, excluding a compensatory up-regulation of this type. We also observed that a combined injection of both MyBPC-2A and MyBPC-2B MOs resulted in a reduction of the MyBPC-2B to a similar extent as that shown in Fig. 2. For the analysis of knockdown of the slow type (MyBPC-1), which has a lower expression, we used qPCR, and Fig. 2 E shows that a specific knockdown by ∼80% of this isoform can be achieved without effects on the fast isoforms.

Altered morphology with aberrant muscle structure in MyBPC-2B morphants

Fig. 3 shows photos of larvae at 4 dpf. Compared with the control-injected larva (Fig. 3 A), neither the MyBPC-1 (Fig. 3 B) nor the MyBPC-2A (Fig. 3 C) morphants revealed any major changes in general morphology. In contrast, the MyBPC-2B morphant (Fig. 3 D) was markedly affected. The translational blocking MyBPC-2B morphants
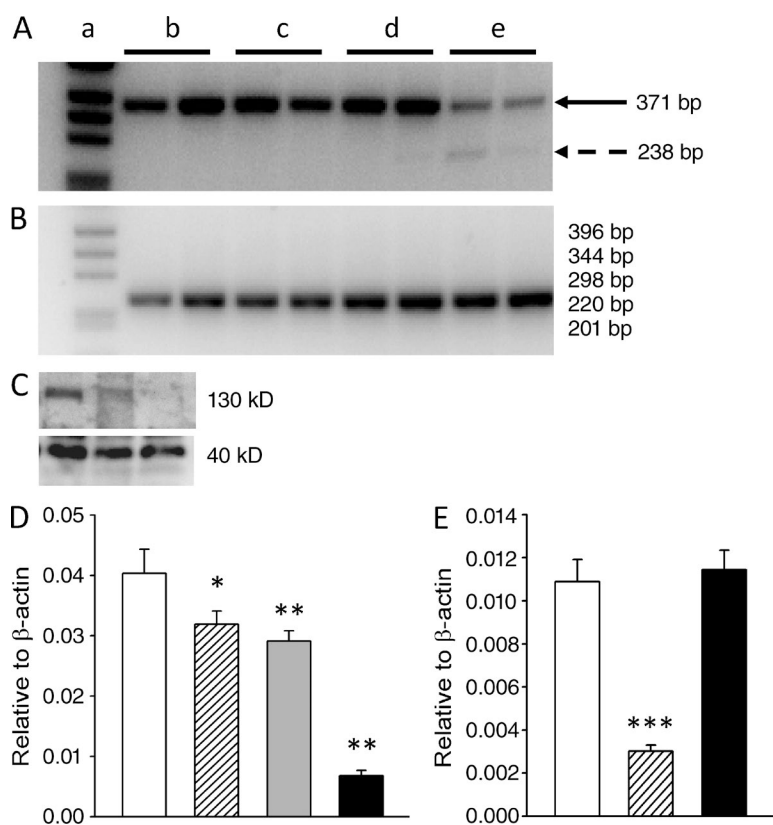

Figure 2. Knockdown of MyBPC expression in 4-dpf larvae. (A) A 2% agarose gel separation of standard (lane a) and of PCR products using primers for *mybpc-2b* (lanes b–e). Two samples from each condition were run in parallel in separate lanes. Samples from control-injected larvae are shown in lane b. Lanes c–e show results from larvae injected with splicing blocking MOs for *mybpc-1*, *mybpc-2a*, and *mybpc-2b* (∼4 ng), respectively. The arrow indicates the main PCR product for *mybpc-2b* (371 bp). The dashed arrow shows an extra PCR product (238 bp) for *mybpc-2b* generated by the splicing MOs. (B) Corresponding PCR products from the same larval materials, using primers for β-actin. Each lane was loaded with extracts from a single larva. The bands in the standards (lane a) in A and B were from above: 506 (not visible in B), 396, 344, 298, 220, and 201 bp. (C) Western blot of protein extracts from the trunk muscles of control and splicing and translational blocking MyBPC-2 morphants (lanes from left to right). The MyBPC-2 bands (molecular mass ∼130 kD) are shown in the top and the corresponding GAPDH bands (molecular mass around 40 kD) in the bottom blots. (D) Summarized data for *mybpc-2b* mRNA expression in control-injected larvae (open bar) and larvae injected with MO for *mybpc-1* (hatched bar), *mybpc-2a* (gray bar), and *mybpc-2b* (black bar); $n = 2$–4. (E) qPCR data for MyBPC-1 expression in control-injected larvae (open bar) and larvae injected with MO for *mybpc-1* (hatched bar) and *mybpc-2b* (black bar); $n = 4$. Results from statistical analysis (ANOVA) are indicated in the figure: *, $P < 0.05$; **, $P < 0.01$; ***, $P < 0.001$. Data are presented as mean ± SEM.

exhibited similar changes in animal morphology relative to their controls (Fig. S3). On average, the MyBPC-2B morphants had a significantly shorter body length (morphants: 2.93 ± 0.04 mm, $n = 5$; control: 3.76 ± 0.04 mm, $n = 5$; P < 0.001), as well as signs of cardiac edema. The cross-sectional area of the skeletal muscle in the central part of the larvae, determined from sample sections, was ∼24% smaller (morphants: [2.94 ± 0.21] × 10^4 μm^2, $n = 5$; controls: [3.87 ± 0.22] × 10^4 μm^2, $n = 6$; P < 0.001). To further examine the structure of MyBPC-2B morphant skeletal muscle, we performed rhodamine phalloidin staining of F-actin in preparations fixed at optimal length for active force generation (L_{opt}; see Fig. 5). In control larvae (Fig. 3 E), the muscle fibers/myofibrils had clear sarcomere patterns and were organized in parallel between the myosepta. In the

MyBPC-2B morphant (Fig. 3 F), the muscle fibers appeared to be thinner and irregular in size with empty space between the fibers/myofibrils. The distribution of sarcomere lengths was wider in the MyBPC-2B morphants (Fig. 3 G) and shifted toward shorter values. The mean sarcomere length in the MyBPC-2B morphants was significantly (P < 0.001) shorter (1.64 ± 0.02 μm, $n = 6$) compared with controls (1.99 ± 0.04 μm, $n = 6$). We estimated the actin filament length from the rhodamine phalloidin–stained images (i.e., 0.5× the length of the rhodamine-stained actin regions) and found a significantly shorter actin filament length (controls: 0.86 ± 0.01; MyBPC-2b morphants: 0.63 ± 0.03 μm; $n = 6$; P < 0.001).

As seen in the micrographs (Fig. 3, E and F), the morphant muscles had more loose arrangement of muscle fibers with some gaps. We estimated the relative gap
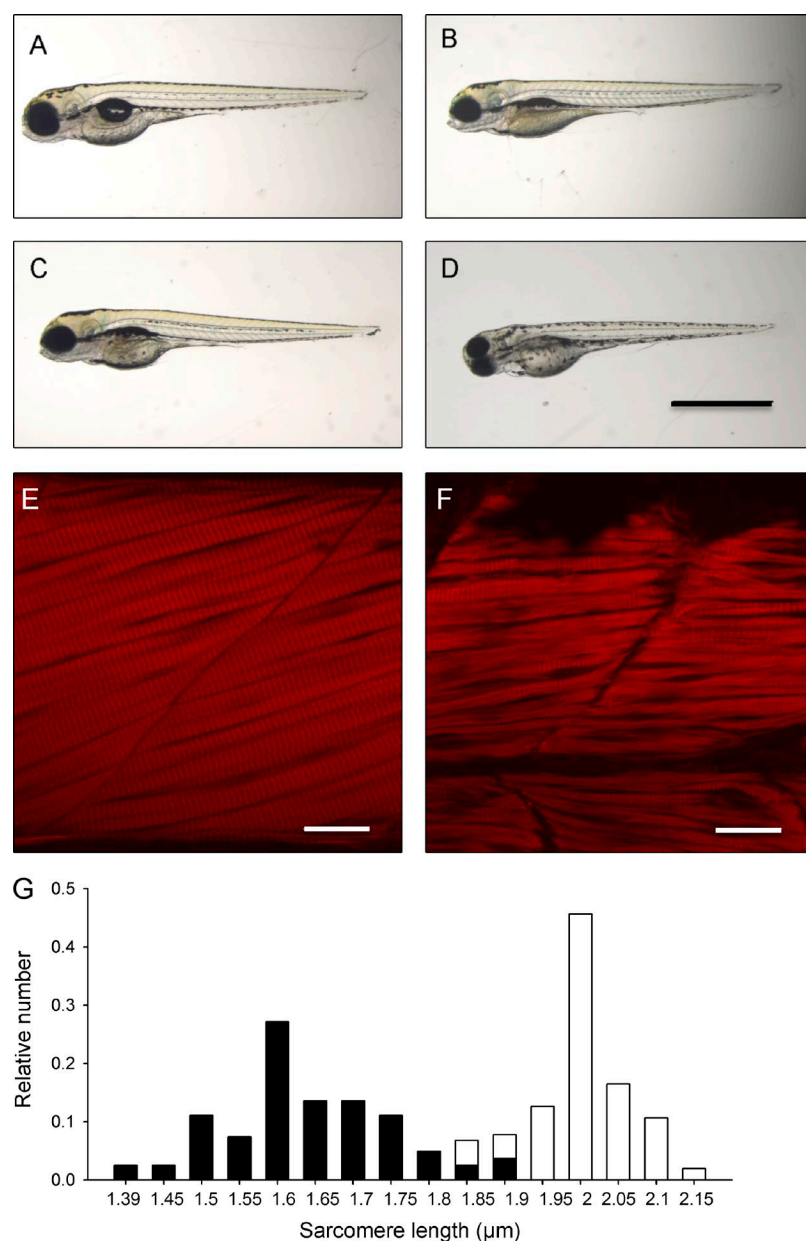
Figure 3. Morphology of control and MyBPC morphants. (A–D) Microscopy of 4-dpf control-injected (A) larva and larvae injected with splicing blocking MOs for *mybpc-1* (B), *mybpc-2a* (C), and *mybpc-2b* (D). (E and F) Confocal microscopy of preparations fixed at optimal length for active force development and stained for F-actin (rhodamine phalloidin) from a control and an MyBPC-2B morphant, respectively. Bars: (A–D) 1.0 mm; (E and F) 20 µm. (G) The relative distribution of sarcomere length at optimal length determined in four fixed preparations from each group (controls: open bars, *mybpc-2b* morphants: black bars). Measurements were grouped and plotted against sarcomere length.

area by placing lines on the images perpendicular to the long axis of the muscles and estimated the relative area (length) of the space between muscle myofibrils. These measurements showed a significantly larger gaps (i.e., lower packing of myofibrils) in the morphants (control: $2.5 \pm 0.1\%$; MyBPC-2B morphants: $12.2 \pm 1\%$; $n = 6$; $P < 0.001$). The mean angle of the myofibrils relative to the preparation long axis was smaller in the morphants (controls: $14.1 \pm 0.6°$; MyBPC-2b morphants: $6.5 \pm 0.6°$; $n = 21–24$; $P < 0.001$).

Elevated apoptosis and increased expression of muscle protein degradation factors in MyBPC-2B morphants

Because the MyBPC-2B morphants were generally smaller with signs of structural defects, we examined whether this group had altered expression levels of key factors in protein degradation. For comparison, we also included MyBPC-1 morphants. Fig. 4 shows expression levels at 4 dpf of myogenin, muscle-specific RING finger proteins (MuRF1–3), microtubule-associated protein 1 light chain 3B (LCB3), and sequestosome 1 (SQSTM1) in skeletal muscles of control-injected larva (open bars), MyBPC-1 morphants (hatched bars), and MyBPC-2B morphants (closed bars). The MuRF1–3 proteins, which are associated with ubiquitination-dependent degradation, were more than twofold elevated in the MyBPC-2B morphants compared with the controls and with the MyBPC-1 morphants. LCB3 and myogenin, associated with protein degradation and regeneration signaling, respectively, were also increased in the MyBPC-2B morphants. The SQSTM1, which interacts with MuRF2, was marginally increased in the MyBPC-2B morphants. Knockdown of the MyBPC-1 type did not change the levels of these transcription factors, except for SQSTM1. Control and MyBPC-2B morphant larvae (1 dpf) were stained with Acridine orange to detect apoptosis. As seen in the confocal images (Fig. 4, inset), the morphants (Fig. 4, inset, right) had an increased number of staining spots in the muscle tissue, indicating elevated apoptosis.

Lower active force and altered length-force relationship in MyBPC-2B morphants

The functional impact of the lack of the MyBPC skeletal isoforms in trunk muscles was investigated in mechanical experiments. Length-force relationships were determined in muscles from 4–6-dpf control and MyBPC morphants. The muscles were stimulated to give single twitch contractions at different lengths. The relationships (Fig. 5 A) were bell-shaped in all groups, and the optimal length (L_{opt}) for active force development could be determined. The sarcomere lengths measured at L_{opt} are given in Fig. 3. Because passive tension increased steeply at lengths above L_{opt} and the preparations often tended to slip and break at longer lengths, we only recorded one point on the descending limb of the length-active force relationship. We have previously shown that the drop in active tension at lengths above L_{opt} is reversible upon return to L_{opt} (Dou et al., 2008). On average, the L_{opt} was reached when the muscles were stretched to ~ 1.3 times of the slack length in all groups. The zebrafish larval muscles most likely operate at the sarcomere length below optimal as discussed previously (Li et al., 2013). The sarcomere lengths determined at L_{opt} in fixed samples of controls and MyBPC-2B morphants are presented in Fig. 3. The ascending limb of the length-active force relationship was left shifted in the MyBPC-2B morphants compared with that in the controls and the MyBPC-1 group. We evaluated the relative length where force was 50% of maximal, and the values in the MyBPC-2B morphants were significantly ($P < 0.05$) lower than in the two other groups (L/L_{opt} at 50% relative force: MyBPC-2B, 0.794 ± 0.017; MyBPC-1, 0.846 ± 0.012; controls, 0.843 ± 0.013; $n = 5–7$), reflecting a less steep ascending limb of the length-force relationship. Fig. 5 B summarizes the active and passive force at L_{opt}
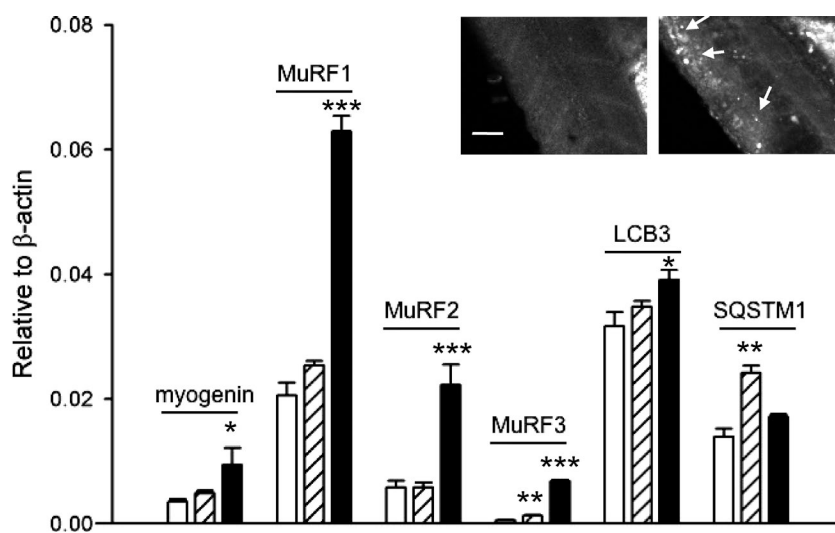
Figure 4. Expression of mRNA for atrophy and protein degradation–associated factors. Larvae (4 dpf) injected with control morpholinos (open bars) or with morpholinos for *mybpc-1* (hatched bars) and *mybpc-2b* (black bars). The qPCR data for muscle-specific RING finger proteins (MuRF1–3), microtubule-associated protein 1 light chain 3B (LCB3), sequestosome 1 (SQSTM1), and myogenin are expressed relative to β-actin levels; $n = 3–4$ in each group. Statistical analyses (ANOVA) are indicated: *, $P < 0.05$; **, $P < 0.01$; ***, $P < 0.001$. (inset) Acridine orange staining of a control (left)- and *mybpc-2b* (right)-injected larvae at 1 dpf. Arrows indicate muscle regions with increased apoptosis. Bar, 50 µm.

in the controls and morphants. The active force of the MyBPC-2B morphants (0.388 ± 0.039 mN) was ~45% of that in the controls (0.861 ± 0.047 mN) and MyBPC-1 morphants (0.878 ± 0.059 mN). A similar decrease in active force was observed in the translation blocking MyBPC-2B morphants (0.368 ± 0.011 mN, $n = 5$). We also observed a slightly higher passive force at L_{opt} in the MyBPC-2B group. This can reflect the extent of stretch required to reach optimal length, but to exclude that the increased passive force in the MyBPC-2B morphants was caused by fibrosis, we stained muscle sections with Sirius red (Fig. S1). No major increase in staining intensity was observed in the MyBPC-2B morphants, excluding a major increase of collagen. Fig. 5 C shows the single twitch force transients in a control and

an MyBPC-2B morphant. As seen in the recordings, the morphant had a lower active force, prolonged time between stimulus and onset of contraction (latency), and slower rates of contraction and relaxation. These parameters are summarized in Fig. 5 D.

Maximal shortening velocity in MyBPC-2B morphants

To explore whether MyBPC-2B affects cross-bridge kinetics, we estimated the maximal shortening velocity in MyBPC-2B morphants and in controls at L_{opt} using iso-velocity ramps. As discussed in the Materials and methods section, the iso-velocity maneuvers were applied during single twitch contractions, caused by the need to estimate shortening velocity during early phases of contraction. Original traces of force responses and velocity
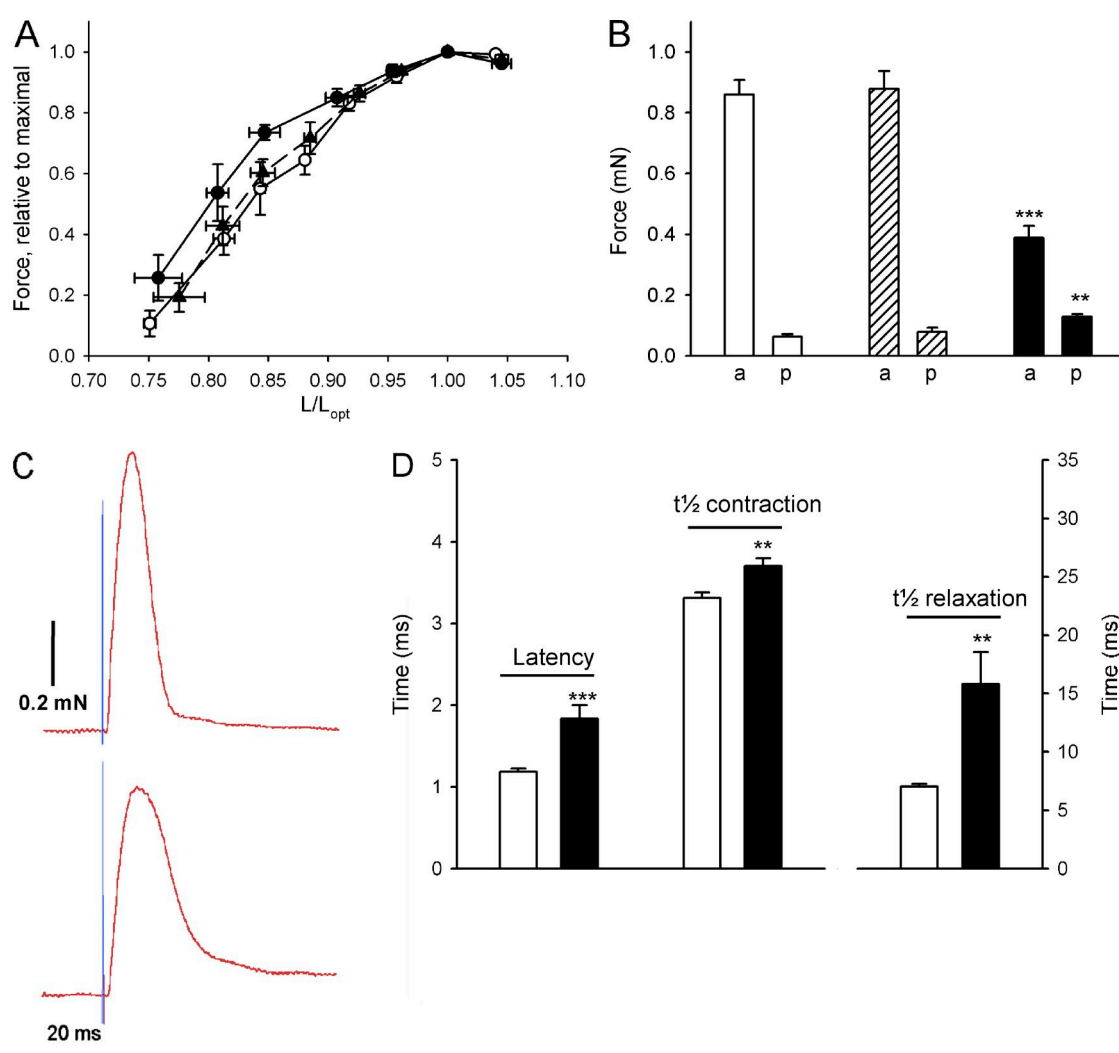
Figure 5. Mechanical properties of control and MyBPC morphants. (A and B) Length–active force relationships (A) and active (a) and passive (p) force at optimal length (B) in skeletal muscles from 4–5-dpf control (open circles and bars) and MyBPC morphants (*mybpc-1*: triangles and hatched bars, *mybpc-2b*: black circles and bars). (C) Original recordings of single twitch contractions from a control (top) and an MyBPC-2B morphant (bottom). The initial rapid transient preceding the force development indicates the stimulation. (D) Summarized data for the latency (i.e., time between stimulus and onset of contraction) and half-time ($t_{1/2}$) for contraction and relaxation during single twitch (open bars: controls [$n = 8$], black bars: MyBPC-2B morphants [$n = 7$]). Statistical analysis: **, P < 0.01; ***, P < 0.001. Data are presented as mean $\pm$ SEM.

ramps are shown in Fig. S2. All velocity values were determined at L_{opt}, and we assume that the Ca^{2+} transients and activation during the twitch were not dramatically affected by the shortening in either group because the time between stimulus and peak of contraction remained the same in isometric and shortening muscles (isometric 12.15 ± 0.14 ms, $n = 6$; shortening at 1 ML/s: 12.23 ± 0.15 ms in controls; isometric 16.58 ± 0.20 ms, $n = 6$; shortening at 1 ML/s: 16.3 ± 0.32 ms in morphants). Force-velocity relationships during single twitch contractions were constructed for each preparation by plotting shortening velocity (V, in muscle lengths/second [ML/s]) against force (P) during shortening. P values were related to the isometric tension (P_0). A hyperbolic equation: $V = b * (1 - P/P_0)/(a/P_0 + P/P_0)$, was fitted to the data with the parameters b and a/P_0 and extrapolated to $P/P_0 = 0$ to obtain the maximal shortening velocity (V_{max}). The relationships were comparatively linear, which most likely reflects the non–steady-state situation during which measurements were made, and we therefore focused on the V_{max} value. The hyperbolic equation was only used for estimating the V_{max}, and the parameters b and a/P_0 were not considered relevant or further analyzed. The V_{max} of the MyBPC-2B morphants in ML/s was ~40% higher and significantly different from that of the controls, as shown by the relationship between V and P/P_0, and the mean V_{max} values (Fig. 6). It should be noted that sarcomere lengths are shorter and with a wider distribution in the MyBPC-2B group (Fig. 3), which makes the extrapolation to the filament
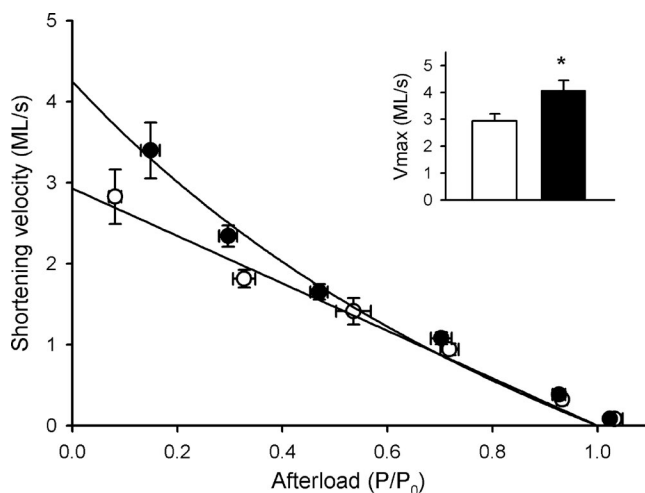
Figure 6. Force-velocity relationships of control and MyBPC morphants. Data from intact trunk muscles during single twitch contractions of controls (open symbols and bar, $n = 6$) and MyBPC-2B morphants (black symbols and bar, $n = 4$). Velocity data were grouped according to afterload, and the mean values are shown in the diagram. A hyperbolic equation (see Results) was fitted to the data and extrapolated to determine the V_{max}. The inset shows the mean V_{max} values determined by fitting the equation to data of individual fibers. *, P < 0.05. Data are presented as mean ± SEM.

level difficult. However, when the maximal velocity of filament sliding (i.e., velocity per half sarcomere) was estimated (ML/s values are multiplied by the mean sarcomere length at L_{opt} from Fig. 3 and divided by two), the difference between control (2.92 ± 0.26 µm half sarcomere/s, $n = 7$) and morphants (3.35 ± 0.31 µm half sarcomere/s, $n = 8$) was smaller (~15%) and not significant, suggesting that lowering the content of MyBPC-2 had only a minor effect on filament sliding velocity. Immunohistochemistry was used to examine the relative proportion of the fast and slow muscle fibers. The fast myosin was expressed predominantly in the inner regions, and the slow myosin was observed in a thin outer layer of the trunk muscles (Fig. S1). No major changes in the relative proportion of the fast and slow muscle components were observed in the MyBPC-2B morphants compared with the controls, showing that velocity was not influenced by a major change in fiber types. The stiffness of the series elastic component ($\Delta P/(Po\Delta L)$) was similar in the two groups (controls: 190.1 ± 21.5; morphants: 208.3 ± 9.7, ML^{-1}, $n = 6$). However, when normalized to mean half sarcomere length, these values became significantly different and would indicate an increased active stiffness in the morphant group (controls: 191 ± 22; morphants: 253 ± 12, $n = 6$; $µm^{-1}$ half sarcomere; P < 0.05).

Wider filament spacing in MyBPC-2B morphants

We obtained strong 1.1 and 1.0 equatorial reflections from control 4-dpf zebrafish larvae (Fig. 7 A). The corresponding reflections in the morphants (Fig. 7 B) were clearly visible, although weaker. At low osmolarity (65 mOsm; Fig. 7 C), the lattice spacing was similar in the two groups. When the osmolarity was increased toward the level in our standard physiological buffered solution (~300 mOsm), the lattice spacing (calculated from the 1.0 reflection, d_{10}) was compressed in both groups, but was markedly wider in the morphants. This difference became more pronounced when the spacing was further compressed by increasing osmolarity in the bathing solution (Fig. 7 C). At optimal stretch of the muscles and at normal osmolarity, significantly wider d_{10} filament spacing was observed in both splicing (39.20 ± 0.42 nm, $n = 10$, P < 0.01) and translation blocking morphants (38.70 ± 0.22 nm, $n = 7$, P < 0.01) compared with the controls (37.26 ± 0.21 nm, $n = 16$). No significant difference was detected between the translation and splicing blocking groups. To further examine lateral anchoring of the contractile filaments and a possible difference in sarcomere volume, the lattice spacing was determined at different degrees of stretch (Fig. 7 D). As seen in the diagram, a shortening of control muscle by ~20% from optimal length (i.e., from a relative stretch of 1.3 to ~1.05), would increase the spacing to about the same level as that in the morphants at optimal length. This is consistent with the

20% shorter sarcomere length at optimal length in the morphants. This suggests that the sarcomeres at optimal length (L_{opt}) are arranged in a shorter but more expanded manner in the MyBPC morphants compared with those of the controls.

To explore whether MyBPC-2B affects the position of the myosin heads in relaxed and contracted conditions, we determined the intensity ratio between the 1.1 and 1.0 reflection as an indication of the mass transfer between thick and thin filaments. As seen in Fig. 7 E, the ratio was similar in controls and MyBPC-2B morphants in the relaxed state. During active tetanic contractions (200 ms, 200 Hz), the intensity ratio increased significantly in the control group. The increase in ratio (from ~0.4 to ~0.7) in the control muscles was comparatively small in relation to the increase observed in rigor (to ~2.3). This most likely reflects that active contractions in the zebrafish muscles involve a comparatively low number of attached cross-bridges. In the MyBPC-2B morphants, the increase in 1.1/1.0 intensity ratio during contraction tended to be smaller than that in the controls (from ~0.5 to ~0.6). The increase in ratio in rigor in the morphants was significantly lower than that of the controls. We confirmed in the MyBPC-2b morphants that longer incubation time in NaCN (60 vs. 45 min) did not increase the intensity ratio further (intensity ratio at 60 min relative to that at 45 min: 0.95 ± 0.09, $n = 4$). If we assume that all cross-bridges attach in rigor and relate the mean values of the 1.1/1.0 intensity ratio (from Fig. 7) in the relaxed state to that in rigor, the results suggest that a larger number of cross-bridges have moved out toward actin in the relaxed state in the morphant group (controls: 0.162 vs. morphants: 0.346). Similar calculation for the active contractions would give a higher relative ratio in the morphant group (controls: 0.303 vs. morphants 0.406).

DISCUSSION

We report that lowering the expression of the fast skeletal MyBPC isoform (MyBPC-2) in zebrafish larvae results in a skeletal myopathy, characterized by muscle weakness and structural changes. This gene is duplicated in the zebrafish, and we find that the MyBPC-2B transcript is the most abundant variant in the larval trunk muscles and that the MyBPC-2A is not expressed or functional at the examined time points. MyBPC-2B is expressed already from 1 dpf, when muscle function is established. The slow type (MyBPC-1) appeared later in the skeletal muscles of the zebrafish, with low expression levels compared with the MyBPC-2B. It has been found using in situ hybridization (Chen et al., 2013) that the cardiac MyBPC-3 is expressed in zebrafish skeletal muscle during early development and decays after ~1–2 dpf. We find that the expression of MyBPC-3 was very low in the trunk muscles compared with that of the skeletal MyBPC isoforms at the later larval stages (1–7 dpf). The function of MyBPC-3 in skeletal muscle is unknown, and it has been shown that knockout of the cardiac MyBPC-3 in the mouse does not affect skeletal muscle (Lin et al., 2013). In view of this study, and the low expression of MyBPC-3 in the trunk muscles, we did not further investigate the role of this isoform in the zebrafish skeletal muscle. Using MO injection, we knocked down the MyBPC-2B and the slow MyBPC-1 expressions by ~80%, as judged by mRNA levels. Our analysis of protein extracts showed a >50% decrease in the MyBPC protein after MyBPC-2B MO injection. Most experiments
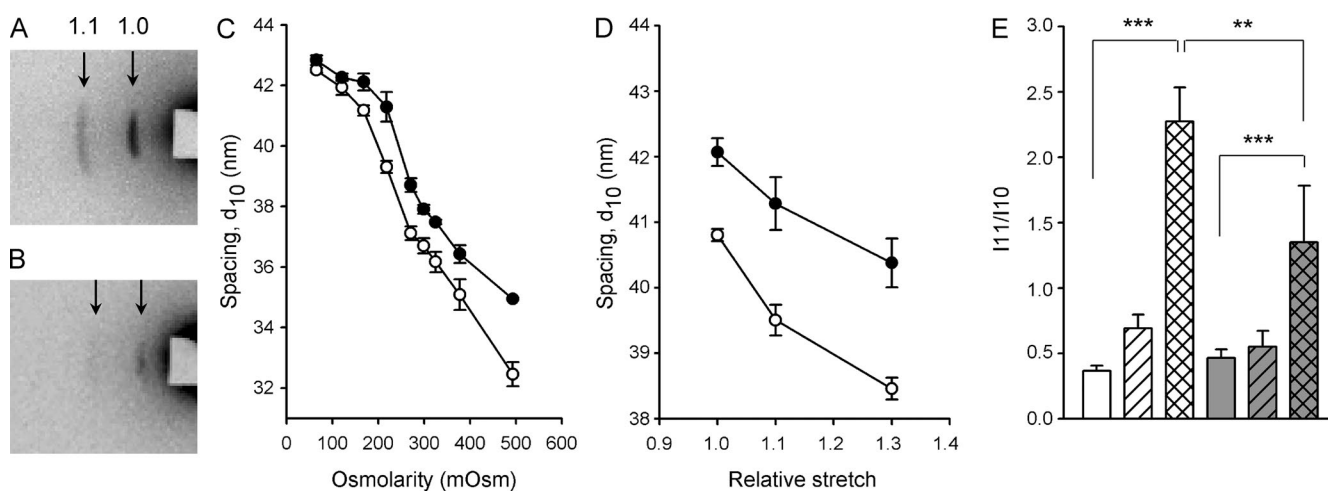
Figure 7. X-ray diffraction of control and MyBPC-2B morphants. (A and B) Patterns from a control (A) and MyBPC-2B morphant (B). Arrows indicate 1.0 and 1.1 reflections. (C) Lattice spacing (d_{10}) at varied osmolarity at optimal length (controls: open symbols, morphants: black symbols). (D) The response to varied stretch (control: open symbols [$n = 6$], morphants: black symbols [$n = 6$]). Stretch is expressed relative to the slack length (1.3 corresponds to the optimal length in both groups). (E) The intensity ratio (I11/I10; controls: open bars, morphants: gray bars; relaxed and contracted states are indicted with nonhatched and hatched bars [$n = 5–6$ in each group]; crossed bars represent the rigor state [$n = 4$]). **, P < 0.01; ***, P < 0.001. Data are presented as mean ± SEM.

were performed using splicing blocking MOs, but the alternative translation blocking of MyBPC-2B gave similar results on gross morphology, active force, and x-ray scattering. The similar results obtained in splicing and translational MyBPC-2B MOs and the lack of effects of control, MyBPC-1, and MyBPC-2A MOs excludes any major off-target effects from the MyBPC-2B MO injection. MyBPC-1 and MyBPC-2 can be coexpressed in the same muscle types in mammals (Gautel et al., 1998), which could suggest some interdependence in their expression. We found no compensation in the other MyBPC isoforms in the MyBPC-1 and 2B morphants, suggesting that these genes are independently regulated. It has been reported that missense mutations in the slow MyBPC-1 in humans are associated with severe skeletal muscle dysfunctions (distal arthrogryposis type 1 myopathy [Gurnett et al., 2010] and autosomal-recessive lethal congenital contractural syndrome [Markus et al., 2012]). Evidence has also been presented that knockdown of MyBPC-1 or overexpression of mutant forms result in myopathy in the zebrafish (Ha et al., 2013). In our experiments, we did not observe any major changes in gross morphology after knockdown by ~80% at the mRNA level of the slow MyBPC-1. We do not know the reason for this difference compared with the study by Ha et al. (2013); it might relate to the strain of zebrafish (AB vs. Tübingen) or the design of the antisense morpholinos, or it might be that a more extensive knockdown is required. We did not find a major functional deficit in single-twitch contractions, suggesting that the contractile function of the trunk muscles is not affected by the extent of MyBPC-1 knockdown achieved in our experiments. However, it can still be possible that more subtle contractile effects are present in the MyBPC-1 morphants. In contrast, the MyBPC-2B morphants exhibited a severe skeletal muscle myopathy with increased apoptosis, altered sarcomeric structure, and impaired contractile function. These changes were accompanied by general changes in the animal morphology, including cardiac edema, most likely secondary to the significant impairment of the skeletal muscle.

The MyBPC-2B myopathy was accompanied by significant activation of striated muscle-specific ring finger proteins (MuRF1–3), which are associated with muscle protein turnover. One of the key up-regulated signaling components, MuRF1, promotes thick filament disassembly (Cohen et al., 2009). The MuRF2 and MuRF3 are proposed to influence the maintenance of the sarcomeric M- and Z-line (McElhinny et al., 2004; Perera et al., 2011). We also observed increased myogenin, implying activation of regeneration processes (Onofre-Oliveira et al., 2012) and morphological signs of elevated apoptosis. Mechanical interactions in the sarcomere mediated via titin and a titin kinase pathway have been shown to activate MuRF signaling (Lange et al., 2005). Mice expressing a variant of MyBPC-3 lacking the titin and myosin-binding domains develop a cardiomyopathy with ultrastructural changes in the sarcomere (Yang et al., 1998). It is possible that a similar mechanism is present in the MyBPC-2 knockdown larvae, that the lack of fast skeletal MyBPC during early skeletal muscle development in the zebrafish affects the mechanical sensing associated with titin and thereby activates MuRF signaling and muscle degeneration.

Although we observed regular cross striations in the MyBPC-2B morphants, the sarcomeres were significantly shorter, with a length inhomogeneity, shorter actin filaments, and a wider interfilament spacing. Further analysis of sarcomere ultrastructure was not the focus of the current study but might give additional information on the role of MyBPC-2 in the assembly of sarcomeres. The shorter sarcomeres were associated with shorter actin filaments, but we do not at present have information on the thick filament structure in the MyBPC-2 morphants. Evidence has previously been presented that cardiac MyBPC-3 together with actin, titin, myomesin, and other sarcomeric partners forms cytoskeletal links guiding thick filament assembly in cardiomyocytes (Van Der Ven et al., 1999; Bhuiyan et al., 2012) and that this process is affected in MyBPC-associated cardiomyopathy (Freiburg and Gautel, 1996). In the cardiac muscle, ablation of MyBPC-3 does not alter the A-band length (Luther et al., 2008), suggesting that removal of this isoform alone does not affect thick filament length in vivo. The slow skeletal MyBPC-1 has been shown to regulate the thick filament assembly via interactions with obscurin (Ackermann et al., 2009). However, our results do not reveal any major effects of knockdown of the slow MyBPC-1 in the zebrafish skeletal muscle, which suggests that sarcomeres can be normally assembled even if the expression of MyBPC-1 is significantly reduced. The role of the fast skeletal MyBPC-2 in filament assembly has not been examined previously, but our results, that the sarcomere structure is affected by MyBPC-2 removal, suggest that this MyBPC type is mandatory for the initial assembly of a normal contractile apparatus with adequate sarcomere lengths and interfilament spacing. We observed a significant expression of MyBPC-1 at 4 dpf. As discussed above in this paragraph, this variant appears not to be required for the muscle function but might have some impact on the structure/function when the fast MyBPC-2 isoform is absent.

MyBPC is located in the C-zone of the sarcomere at a periodicity of ~43 nm (Rome et al., 1973; Luther et al., 2008) with close interactions with other proteins. It has been shown that the cardiac MyBPC in the sarcomere affects cross-bridge force production; the cross-bridges in the C-zone (with MyBPC) generate higher active force (Wang et al., 2014). The localization of MyBPC-2 in the zebrafish fast striated muscles is not known. It is, however, expected that lack of this protein would affect both muscle function and sarcomeric structure. In the

current study, we focused on the equatorial reflections in the small-angle x-ray scattering patterns, giving information on the lateral dimensions of the filament lattice. The wider spacing in the MyBPC-2B morphants shows that the protein is required for maintenance of the distance between the contractile filaments in the skeletal muscle. Because the optimal sarcomere length for active force was shorter in the morphants, the wider spacing is not simply caused by a reduced stretch of the sarcomeres, but rather reflects a primary alteration in sarcomere structure. The wider spacing is consistent with a study of the cardiac muscle from MyBPC-3 knockout mice (Colson et al., 2007), where the lattice spacing tended to be wider. In contrast, Palmer et al. (2004) reported no significant difference, and Palmer et al. (2011) even showed a reduced spacing in an effective MyBPC-3–null model. Our data from the zebrafish support a prominent role of MyBPC-2 in maintaining the filament arrangement in the skeletal muscle sarcomere. It has been suggested that the protein via interaction with actin regulates the organization of the myosin heads and the thick filament backbone (Reconditi et al., 2014). If the protein introduces a mechanical link between filaments, it must be assumed that the binding is sufficiently weak not to inhibit filament sliding during shortening or that it is weakened during activation. MyBPC affects the tropomyosin position and the Ca^{2+} sensitivity (Luther and Craig, 2011; Mun et al., 2014), which might suggest that thin filament activation during active contraction also weakens the MyBPC–thin filament interactions to enable filament sliding.

We determined the equatorial 1.1/1.0 intensity ratio, which reflects the mass transfer between contractile filaments (Millman, 1998). It has been shown that lack of MyBPC-3 in cardiac muscle results in a 30% increase in this ratio (Colson et al., 2007), suggesting that MyBPC has a role in restraining the myosin heads to the thick filaments. We did not observe any significant change in the 1.1/1.0 intensity ratio in the relaxed state, between controls and morphants. However, the intensity increase in rigor was significantly lower in the morphant group. We show that the time in NaCN was sufficient to generate a stable change in 1.1/1.0 ratio. When the relaxed pattern is related to the rigor values, it will be higher in the morphant group. Although, the assumption that 100% of cross-bridges are attached in rigor must be regarded with caution, the results would be consistent with an increased transfer of myosin heads toward actin in the relaxed state after knockdown of MyBPC-2B. This finding is consistent with a role of MyBPC-2 affecting the position of the myosin heads in relation to the thick filament backbone, similar to the function proposed for MyBPC-3 (Winegrad, 1999). It should be noted that the skeletal MyBPC-2 lacks some of the phosphorylation sites, which regulate the MyBPC-3/myosin interactions and the radial cross-bridge movement in the cardiac

system (Winegrad, 1999). Thus, such an effect on cross-bridge positioning by MyBPC-2 would be occurring in the absence of this regulatory mechanism.

The active contractions at optimal length were significantly weaker in the MyBPC-2B morphants compared with that of the controls. Several factors might be involved, including (a) the decreased cross-sectional area of the trunk muscles, most likely as the result of impaired structural development or muscle degeneration, (b) the shorter sarcomere length and wider length distribution resulting in fewer parallel coupled contractile units, (c) faster cross-bridge cycling, (d) lower force per cross-bridge, or (e) altered activation properties. Regarding a, the decrease in cross-sectional area ($\sim$24%) and the increase in gaps between muscle fibers in the MyBPC-2B morphants were smaller than the decrease in active force ($\sim$55%), suggesting that a smaller muscle size is not the sole explanation for the lower force generation. An increase in interfilament spacing of the magnitude observed in the MyBPC-2 morphants would not affect force generation, as shown previously (Li et al., 2013). Because the direction of the myofibrils is mainly along the long axis of the preparations, the orientation of muscle fibers would not affect the force generation. Regarding b and e, the leftward shift of the ascending part of the active length-force curve could be a reflection of a sarcomere inhomogeneity. It should be noted that the structural basis of the ascending limb is complex and that the morphants were weaker and had a different sarcomere length distribution, thus making interpretation of this result difficult. However, the finding is consistent with a model where MyBPC-2B has a role in determining the length dependency of the active force at short lengths, possibly by affecting the Ca^{2+} sensitivity of the thin filament regulatory system (Luther and Craig, 2011; Mun et al., 2014). Regarding c, although faster cycling rate theoretically could decrease cross-bridge duty cycle and active force, the shortening velocity at the filament level does not suggest a major difference in cross-bridge cycling rate after MyBPC-2 removal. Regarding d, it has been suggested that cross-bridges in cardiac muscle lacking MyBPC-3 produce lower active force (Wang et al., 2014), which might apply also for the skeletal muscle. We observed a slower relaxation in the MyBPC-2 morphants, which could reflect the inhomogeneities in the sarcomere length distribution, changes in Ca^{2+} handling, or direct effects of MyBPC-2 on the cross-bridge detachment process during relaxation.

Because previous studies have suggested that MyBPC influences striated muscle shortening velocity (Hofmann et al., 1991a; Korte et al., 2003), we estimated the maximal shortening velocity (V_{max}) during rapid single twitch contractions of the zebrafish muscles and showed that knockdown of MyBPC-2B increased the V_{max} by $\sim$40%. It should be stated that these measurements were performed under non–steady-state conditions, which

makes the determination of the full force-velocity curve difficult. A contributing factor for the higher V_{max} can be that the sarcomere lengths are shorter in the MyBPC-2B morphants. This change would increase the V_{max} when determined in muscle lengths/second. The exact magnitude of the difference in V_{max} between control and morphants is therefore difficult to estimate, but our study suggests an $\sim15\%$ increase, possibly reflecting a faster cross-bridge turnover after MyBPC-2 removal. Because the relative content of fast and slow skeletal muscle types was not altered, we exclude an effect caused by a fiber type shift. Previous work using skinned skeletal muscle fibers where MyBPC-2 has been partially extracted (Hofmann et al., 1991b), from MyBPC-3 knockout mice and from in vitro motility assays (Korte et al., 2003; Saber et al., 2008), has suggested that MyBPC slows cross-bridge cycling, possibly via introduction of an internal load or direct effects on the actin–myosin interaction. Our results are consistent with these findings and show that the fast MyBPC-2 slows down cross-bridge cycling in the living fibers, albeit to a comparatively small extent.

During the active contraction, cross-bridges in the zebrafish muscle move out toward actin, as shown by the increase in the equatorial 1.1/1.0 intensity ratio (Fig. 7; Dou et al., 2008). This increase in ratio is significantly smaller compared with that observed in contracting frog muscles (Haselgrove and Huxley, 1973) and suggests that a comparatively small fraction of the cross-bridges are attached during contraction in the zebrafish trunk muscles. This most likely reflects a high rate of cross-bridge cycling in the zebrafish muscles, where a rapid detachment of myosin heads leads to a high shortening velocity, but with fewer attached cross-bridges at each instance of time, i.e., a low duty cycle (Rome et al., 1999). This partly explains the comparatively low active force and poor development of tetanic tension in the zebrafish striated muscles. As discussed above in this paragraph, the 1.1/1.0 intensity ratio data from the x-ray diffraction experiments might suggest that cross-bridges in the relaxed state are positioned closer to the actin filaments in the morphants. The intensity ratio value during contraction relative to that in rigor is also higher in the morphants compared with that in the controls, which could be consistent with the higher stiffness value when corrected for the sarcomere length.

The MyBPC-2–associated skeletal muscle myopathy in the zebrafish larvae shares several properties with the cardiac form in mammals, including altered muscle structure, increased rate of cross-bridge cycling, and lower active force. In comparison with MyBPC-3, MyBPC-2 lacks the N-terminal C0 domain and several key regulatory phosphorylation sites. Similar properties of the cardiac and skeletal myopathies can be explained by the common structural properties between the MyBPC-2 and MyBPC-3 isoforms, including several interactions in the sarcomere. However, there is a more prominent effect on sarcomere structure after knockdown of MyBPC-2, suggesting that the skeletal isoform is also required for normal sarcomere establishment. Hitherto, mutations in fast skeletal MyBPC have not been found in human myopathies. However, our findings indicate that MyBPC-2 may be a candidate gene for myopathies of unknown genetic cause.

In conclusion, we find that partial loss of the fast skeletal MyBPC in the zebrafish leads to a severe skeletal muscle myopathy, characterized by general structural defects with apoptosis and with sarcomeric abnormalities. The muscle function is significantly impaired with lower active force and altered length-force behavior.

REFERENCES

Ackermann, M.A., and A. Kontrogianni-Konstantopoulos. 2011. Myosin binding protein-C slow is a novel substrate for protein kinase A (PKA) and C (PKC) in skeletal muscle. *J. Proteome Res.* 10:4547–4555. http://dx.doi.org/10.1021/pr200355w

Ackermann, M.A., L.Y. Hu, A.L. Bowman, R.J. Bloch, and A. Kontrogianni-Konstantopoulos. 2009. Obscurin interacts with a novel isoform of MyBP-C slow at the periphery of the sarcomeric M-band and regulates thick filament assembly. *Mol. Biol. Cell.* 20:2963–2978. http://dx.doi.org/10.1091/mbc.E08-12-1251

Bennett, P.M., D.O. Fürst, and M. Gautel. 1999. The C-protein (myosin binding protein C) family: regulators of contraction and sarcomere formation? *Rev. Physiol. Biochem. Pharmacol.* 138:203–234. http://dx.doi.org/10.1007/BFb0119628

Bhuiyan, M.S., J. Gulick, H. Osinska, M. Gupta, and J. Robbins. 2012. Determination of the critical residues responsible for cardiac myosin binding protein C's interactions. *J. Mol. Cell. Cardiol.* 53:838–847. http://dx.doi.org/10.1016/j.yjmcc.2012.08.028

Bonne, G., L. Carrier, J. Bercovici, C. Cruaud, P. Richard, B. Hainque, M. Gautel, S. Labeit, M. James, J. Beckmann, et al. 1995. Cardiac myosin binding protein-C gene splice acceptor site mutation is associated with familial hypertrophic cardiomyopathy. *Nat. Genet.* 11:438–440. http://dx.doi.org/10.1038/ng1295-438

Chen, Y.H., C.W. Pai, S.W. Huang, S.N. Chang, L.Y. Lin, F.T. Chiang, J.L. Lin, J.J. Hwang, and C.T. Tsai. 2013. Inactivation of Myosin binding protein C homolog in zebrafish as a model for human

cardiac hypertrophy and diastolic dysfunction. *J. Am. Heart Assoc.* 2:e000231. http://dx.doi.org/10.1161/JAHA.113.000231

Cohen, S., J.J. Brault, S.P. Gygi, D.J. Glass, D.M. Valenzuela, C. Gartner, E. Latres, and A.L. Goldberg. 2009. During muscle atrophy, thick, but not thin, filament components are degraded by MuRF1-dependent ubiquitylation. *J. Cell Biol.* 185:1083–1095. http://dx.doi.org/10.1083/jcb.200901052

Colson, B.A., T. Bekyarova, D.P. Fitzsimons, T.C. Irving, and R.L. Moss. 2007. Radial displacement of myosin cross-bridges in mouse myocardium due to ablation of myosin binding protein-C. *J. Mol. Biol.* 367:36–41. http://dx.doi.org/10.1016/j.jmb.2006.12.063

Colson, B.A., I.N. Rybakova, E. Prochniewicz, R.L. Moss, and D.D. Thomas. 2012. Cardiac myosin binding protein-C restricts intrafilament torsional dynamics of actin in a phosphorylation-dependent manner. *Proc. Natl. Acad. Sci. USA.* 109:20437–20442. http://dx.doi.org/10.1073/pnas.1213027109

Craig, R., and G. Offer. 1976. The location of C-protein in rabbit skeletal muscle. *Proc. R. Soc. Lond. B Biol. Sci.* 192:451–461. http://dx.doi.org/10.1098/rspb.1976.0023

Dou, Y., M. Andersson-Lendahl, and A. Arner. 2008. Structure and function of skeletal muscle in zebrafish early larvae. *J. Gen. Physiol.* 131:445–453. http://dx.doi.org/10.1085/jgp.200809982

Edman, K.A. 1979. The velocity of unloaded shortening and its relation to sarcomere length and isometric force in vertebrate muscle fibres. *J. Physiol.* 291:143–159. http://dx.doi.org/10.1113/jphysiol.1979.sp012804

Finley, N.L., and T.I. Cuperman. 2014. Cardiac myosin binding protein-C: a structurally dynamic regulator of myocardial contractility. *Pflugers Arch.* 466:433–438. http://dx.doi.org/10.1007/s00424-014-1451-0

Freiburg, A., and M. Gautel. 1996. A molecular map of the interactions between titin and myosin-binding protein C. Implications for sarcomeric assembly in familial hypertrophic cardiomyopathy. *Eur. J. Biochem.* 235:317–323. http://dx.doi.org/10.1111/j.1432-1033.1996.00317.x

Fürst, D.O., U. Vinkemeier, and K. Weber. 1992. Mammalian skeletal muscle C-protein: purification from bovine muscle, binding to titin and the characterization of a full-length human cDNA. *J. Cell Sci.* 102:769–778.

Furutani-Seiki, M., Y.J. Jiang, M. Brand, C.P. Heisenberg, C. Houart, D. Beuchle, F.J. van Eeden, M. Granato, P. Haffter, M. Hammerschmidt, et al. 1996. Neural degeneration mutants in the zebrafish, Danio rerio. *Development.* 123:229–239.

Gautel, M., O. Zuffardi, A. Freiburg, and S. Labeit. 1995. Phosphorylation switches specific for the cardiac isoform of myosin binding protein-C: a modulator of cardiac contraction? *EMBO J.* 14:1952–1960.

Gautel, M., D.O. Fürst, A. Cocco, and S. Schiaffino. 1998. Isoform transitions of the myosin binding protein C family in developing human and mouse muscles: lack of isoform transcomplementation in cardiac muscle. *Circ. Res.* 82:124–129. http://dx.doi.org/10.1161/01.RES.82.1.124

Gilbert, R., J.A. Cohen, S. Pardo, A. Basu, and D.A. Fischman. 1999. Identification of the A-band localization domain of myosin binding proteins C and H (MyBP-C, MyBP-H) in skeletal muscle. *J. Cell Sci.* 112:69–79.

Gruen, M., H. Prinz, and M. Gautel. 1999. cAPK-phosphorylation controls the interaction of the regulatory domain of cardiac myosin binding protein C with myosin-S2 in an on-off fashion. *FEBS Lett.* 453:254–259. http://dx.doi.org/10.1016/S0014-5793(99)00727-9

Gurnett, C.A., D.M. Desruisseau, K. McCall, R. Choi, Z.I. Meyer, M. Talerico, S.E. Miller, J.S. Ju, A. Pestronk, A.M. Connolly, et al. 2010. Myosin binding protein C1: a novel gene for autosomal dominant distal arthrogryposis type 1. *Hum. Mol. Genet.* 19:1165–1173. http://dx.doi.org/10.1093/hmg/ddp587

Ha, K., J.G. Buchan, D.M. Alvarado, K. McCall, A. Vydyanath, P.K. Luther, M.I. Goldsmith, M.B. Dobbs, and C.A. Gurnett. 2013. MYBPC1 mutations impair skeletal muscle function in zebrafish models of arthrogryposis. *Hum. Mol. Genet.* 22:4967–4977. http://dx.doi.org/10.1093/hmg/ddt344

Harris, S.P., C.R. Bartley, T.A. Hacker, K.S. McDonald, P.S. Douglas, M.L. Greaser, P.A. Powers, and R.L. Moss. 2002. Hypertrophic cardiomyopathy in cardiac myosin binding protein-C knockout mice. *Circ. Res.* 90:594–601. http://dx.doi.org/10.1161/01.RES.0000012222.70819.64

Harris, S.P., E. Rostkova, M. Gautel, and R.L. Moss. 2004. Binding of myosin binding protein-C to myosin subfragment S2 affects contractility independent of a tether mechanism. *Circ. Res.* 95:930–936. http://dx.doi.org/10.1161/01.RES.0000147312.02673.56

Haselgrove, J.C., and H.E. Huxley. 1973. X-ray evidence for radial cross-bridge movement and for the sliding filament model in actively contracting skeletal muscle. *J. Mol. Biol.* 77:549–568. http://dx.doi.org/10.1016/0022-2836(73)90222-2

Hofmann, P.A., M.L. Greaser, and R.L. Moss. 1991a. C-protein limits shortening velocity of rabbit skeletal muscle fibres at low levels of Ca^{2+} activation. *J. Physiol.* 439:701–715. http://dx.doi.org/10.1113/jphysiol.1991.sp018689

Hofmann, P.A., H.C. Hartzell, and R.L. Moss. 1991b. Alterations in Ca2+ sensitive tension due to partial extraction of C-protein from rat skinned cardiac myocytes and rabbit skeletal muscle fibers. *J. Gen. Physiol.* 97:1141–1163. http://dx.doi.org/10.1085/jgp.97.6.1141

Korte, F.S., K.S. McDonald, S.P. Harris, and R.L. Moss. 2003. Loaded shortening, power output, and rate of force redevelopment are increased with knockout of cardiac myosin binding protein-C. *Circ. Res.* 93:752–758. http://dx.doi.org/10.1161/01.RES.0000096363.85588.9A

Kulikovskaya, I., G. McClellan, R. Levine, and S. Winegrad. 2003. Effect of extraction of myosin binding protein C on contractility of rat heart. *Am. J. Physiol. Heart Circ. Physiol.* 285:H857–H865. http://dx.doi.org/10.1152/ajpheart.00841.2002

Kunst, G., K.R. Kress, M. Gruen, D. Uttenweiler, M. Gautel, and R.H. Fink. 2000. Myosin binding protein C, a phosphorylation-dependent force regulator in muscle that controls the attachment of myosin heads by its interaction with myosin S2. *Circ. Res.* 86:51–58. http://dx.doi.org/10.1161/01.RES.86.1.51

Lange, S., F. Xiang, A. Yakovenko, A. Vihola, P. Hackman, E. Rostkova, J. Kristensen, B. Brandmeier, G. Franzen, B. Hedberg, et al. 2005. The kinase domain of titin controls muscle gene expression and protein turnover. *Science.* 308:1599–1603. http://dx.doi.org/10.1126/science.1110463

Li, M., M. Andersson-Lendahl, T. Sejersen, and A. Arner. 2013. Knockdown of desmin in zebrafish larvae affects interfilament spacing and mechanical properties of skeletal muscle. *J. Gen. Physiol.* 141:335–345. http://dx.doi.org/10.1085/jgp.201210915

Lin, B., S. Govindan, K. Lee, P. Zhao, R. Han, K.E. Runte, R. Craig, B.M. Palmer, and S. Sadayappan. 2013. Cardiac myosin binding protein-C plays no regulatory role in skeletal muscle structure and function. *PLoS One.* 8:e69671. http://dx.doi.org/10.1371/journal.pone.0069671

Luther, P.K., and R. Craig. 2011. Modulation of striated muscle contraction by binding of myosin binding protein C to actin. *BioArchitecture.* 1:277–283. http://dx.doi.org/10.4161/bioa.1.6.19341

Luther, P.K., P.M. Bennett, C. Knupp, R. Craig, R. Padrón, S.P. Harris, J. Patel, and R.L. Moss. 2008. Understanding the organisation and role of myosin binding protein C in normal striated muscle by comparison with MyBP-C knockout cardiac muscle. *J. Mol. Biol.* 384:60–72. http://dx.doi.org/10.1016/j.jmb.2008.09.013

Markus, B., G. Narkis, D. Landau, R.Z. Birk, I. Cohen, and O.S. Birk. 2012. Autosomal recessive lethal congenital contractural syndrome

type 4 (LCCS4) caused by a mutation in MYBPC1. *Hum. Mutat.* 33:1435–1438. http://dx.doi.org/10.1002/humu.22122

McElhinny, A.S., C.N. Perry, C.C. Witt, S. Labeit, and C.C. Gregorio. 2004. Muscle-specific RING finger-2 (MURF-2) is important for microtubule, intermediate filament and sarcomeric M-line maintenance in striated muscle development. *J. Cell Sci.* 117:3175–3188. http://dx.doi.org/10.1242/jcs.01158

Michalek, A.J., J.W. Howarth, J. Gulick, M.J. Previs, J. Robbins, P.R. Rosevear, and D.M. Warshaw. 2013. Phosphorylation modulates the mechanical stability of the cardiac myosin-binding protein C motif. *Biophys. J.* 104:442–452. http://dx.doi.org/10.1016/j.bpj.2012.12.021

Millman, B.M. 1998. The filament lattice of striated muscle. *Physiol. Rev.* 78:359–391.

Mun, J.Y., M.J. Previs, H.Y. Yu, J. Gulick, L.S. Tobacman, S. Beck Previs, J. Robbins, D.M. Warshaw, and R. Craig. 2014. Myosin-binding protein C displaces tropomyosin to activate cardiac thin filaments and governs their speed by an independent mechanism. *Proc. Natl. Acad. Sci. USA.* 111:2170–2175. http://dx.doi.org/10.1073/pnas.1316001111

Oakley, C.E., B.D. Hambly, P.M. Curmi, and L.J. Brown. 2004. Myosin binding protein C: structural abnormalities in familial hypertrophic cardiomyopathy. *Cell Res.* 14:95–110. http://dx.doi.org/10.1038/sj.cr.7290208

Offer, G., C. Moos, and R. Starr. 1973. A new protein of the thick filaments of vertebrate skeletal myofibrils: Extractions, purification and characterization. *J. Mol. Biol.* 74:653–676. http://dx.doi.org/10.1016/0022-2836(73)90055-7

Onofre-Oliveira, P.C., A.L. Santos, P.M. Martins, D. Ayub-Guerrieri, and M. Vainzof. 2012. Differential expression of genes involved in the degeneration and regeneration pathways in mouse models for muscular dystrophies. *Neuromolecular Med.* 14:74–83. http://dx.doi.org/10.1007/s12017-012-8172-3

Palmer, B.M., B.K. McConnell, G.H. Li, C.E. Seidman, J.G. Seidman, T.C. Irving, N.R. Alpert, and D.W. Maughan. 2004. Reduced cross-bridge dependent stiffness of skinned myocardium from mice lacking cardiac myosin binding protein-C. *Mol. Cell. Biochem.* 263:73–80. http://dx.doi.org/10.1023/B:MCBI.0000041849.60591.45

Palmer, B.M., S. Sadayappan, Y. Wang, A.E. Weith, M.J. Previs, T. Bekyarova, T.C. Irving, J. Robbins, and D.W. Maughan. 2011. Roles for cardiac MyBP-C in maintaining myofilament lattice rigidity and prolonging myosin cross-bridge lifetime. *Biophys. J.* 101:1661–1669. http://dx.doi.org/10.1016/j.bpj.2011.08.047

Perera, S., M.R. Holt, B.S. Mankoo, and M. Gautel. 2011. Developmental regulation of MURF ubiquitin ligases and autophagy proteins nbr1, p62/SQSTM1 and LC3 during cardiac myofibril assembly and turnover. *Dev. Biol.* 351:46–61. http://dx.doi.org/10.1016/j.ydbio.2010.12.024

Reconditi, M., E. Brunello, L. Fusi, M. Linari, M.F. Martinez, V. Lombardi, M. Irving, and G. Piazzesi. 2014. Sarcomere-length de-pendence of myosin filament structure in skeletal muscle fibres of the frog. *J. Physiol.* 592:1119–1137. http://dx.doi.org/10.1113/jphysiol.2013.267849

Rome, E., G. Offer, and F.A. Pepe. 1973. X-ray diffraction of muscle labelled with antibody to C-protein. *Nat. New Biol.* 244:152–154. http://dx.doi.org/10.1038/newbio244152a0

Rome, L.C., C. Cook, D.A. Syme, M.A. Connaughton, M. Ashley-Ross, A. Klimov, B. Tikunov, and Y.E. Goldman. 1999. Trading force for speed: why superfast crossbridge kinetics leads to su-perlow forces. *Proc. Natl. Acad. Sci. USA.* 96:5826–5831. http://dx.doi.org/10.1073/pnas.96.10.5826

Saber, W., K.J. Begin, D.M. Warshaw, and P. VanBuren. 2008. Cardiac myosin binding protein-C modulates actomyosin binding and kinetics in the in vitro motility assay. *J. Mol. Cell. Cardiol.* 44:1053–1061. http://dx.doi.org/10.1016/j.yjmcc.2008.03.012

Sadayappan, S., J. Gulick, H. Osinska, L.A. Martin, H.S. Hahn, G.W. Dorn II, R. Klevitsky, C.E. Seidman, J.G. Seidman, and J. Robbins. 2005. Cardiac myosin-binding protein-C phosphoryla-tion and cardiac function. *Circ. Res.* 97:1156–1163. http://dx.doi.org/10.1161/01.RES.0000190605.79013.4d

Van Der Ven, P.F., E. Ehler, J.C. Perriard, and D.O. Fürst. 1999. Thick filament assembly occurs after the formation of a cytoskel-etal scaffold. *J. Muscle Res. Cell Motil.* 20:569–579. http://dx.doi.org/10.1023/A:1005569225773

Wang, L., S. Sadayappan, and M. Kawai. 2014. Cardiac myosin binding protein C phosphorylation affects cross-bridge cycle's elementary steps in a site-specific manner. *PLoS One.* 9:e113417. http://dx.doi.org/10.1371/journal.pone.0113417

Watkins, H., D. Conner, L. Thierfelder, J.A. Jarcho, C. MacRae, W.J. McKenna, B.J. Maron, J.G. Seidman, and C.E. Seidman. 1995. Mutations in the cardiac myosin binding protein-C gene on chro-mosome 11 cause familial hypertrophic cardiomyopathy. *Nat. Genet.* 11:434–437. http://dx.doi.org/10.1038/ng1295-434

Weisberg, A., and S. Winegrad. 1996. Alteration of myosin cross bridges by phosphorylation of myosin-binding protein C in car-diac muscle. *Proc. Natl. Acad. Sci. USA.* 93:8999–9003. http://dx.doi.org/10.1073/pnas.93.17.8999

Westerfield, M. 2000. The zebrafish book: A guide for the laboratory use of zebrafish (*Danio rerio*). Fourth edition. Univ. of Oregon Press, Eugene, OR., Available at https://zfin.org/zf_info/zfbook/zfbk.html

Winegrad, S. 1999. Cardiac myosin binding protein C. *Circ. Res.* 84:1117–1126. http://dx.doi.org/10.1161/01.RES.84.10.1117

Witt, C.C., B. Gerull, M.J. Davies, T. Centner, W.A. Linke, and L. Thierfelder. 2001. Hypercontractile properties of cardiac muscle fibers in a knock-in mouse model of cardiac myosin-binding pro-tein-C. *J. Biol. Chem.* 276:5353–5359. http://dx.doi.org/10.1074/jbc.M008691200

Yang, Q., A. Sanbe, H. Osinska, T.E. Hewett, R. Klevitsky, and J. Robbins. 1998. A mouse model of myosin binding protein C human familial hypertrophic cardiomyopathy. *J. Clin. Invest.* 102:1292–1300. http://dx.doi.org/10.1172/JCI3880